Analysis of the April 2005 proton test data

Martin Groenewegen (ICC KUL)
&
Pierre Royer (ICC KUL)

DOCUMENT CHANGE RECORD

Version	Date	Changes	Remarks
Draft 0	05-July-2005	–	start of document
Draft 1	06-December-2005	all	released to PACS-ICC
Draft 2	03-April-2006	Table 8	S/N added

Reference Documents

RD 1 – Test Plan and procedure for investigation of glitch event rate and collected charge variation in the Ge:Ga detectors during proton irradiation at UCL-CRC (2nd test phase, PACS-ME-TP-009, issue 2.2, 5 May 2005, Katterloher, Barl & Schubert
RD 2 – Sixpack data analysis: S/N related issues, PICC-KL-TN-008, P. Royer, Version 1, 28-March-2004
RD 3 – Fitting PACS ramps with analytical models. Part III: The IMEC model, PICC-KL-TN-010, M.A.T. Groenewegen, Sept. 2005
RD 4 – Testing Glitch Detection Algorithms by Monte-Carlo Simulations, PICC-KL-TN-019, Groenewegen et al.
RD 5 – UCL-CRC Proton tests of March 2004: glitch height distribution, PICC-KL-TN-012, M.A.T. Groenewegen (KUL)

1. Introduction

This report focuses on the second phase of the proton irradiation tests which took place in the cyclotron at Louvain-La-Neuve (UCL-CRC) in April 2005, and which is described in RD 1.

Discussed are however not only issues related to glitches and the effect of radiations but also on the pre-irradiation data as this is the first time there is data available on the FM generation of CREs.

2. Integrated versus post-integration noise

The files listed in Table 1 were investigated, which were most pre-irradiation (N1-N16, L1) For each file only detectors 3 and 12 were looked at, as being representative for the case with and w/o the FIR cut-on filter in front.

Each file/detector combination contains 256 ramps of 256 read-outs. The mean voltage at the first read-out over the 256 ramps is subtracted from all ramps (not doing this has no influence on the outcome). At every readout the standard deviation, σ, is determined over all 256 ramps in the dataset. Figure 1 shows a representative plot of how the noise develops as a function of read-out for the highest and lowest bias settings.

The prediction is that the noise would go like: $\sigma^2 = (\sigma_p)^2 + j\ (\sigma_i)^2$ as a function of read-out j, where σ_p and σ_i are the post-integration and integrated noise, respectively. This model was fitted to the data, and the results are listed in Table 1. The post-integration noise is found to be 10-30 times larger than the integrated noise.

Previously, it was found (RD 2) that in a Sixpack data set with 50 mV bias, 0.3 pF capacitance, the post-integration noise was 267. 10^{-5} and the integrated noise 86. 10^{-6} V. This result suggest that the post-integration noise is not significantly reduced compared to the old generation of CREs.

There are some interesting correlations. The post-integration noise is about 10-20% smaller for the larger flux (detector 12) independent of bias. The integrated noise shows more clear correlations: it is smaller for lower bias voltages, and smaller for lower flux-levels.

For a bias of 70 mV the analysis has been repeated for different reset-lengths ($1s$ to $0.125s$). The integrated noise is essentially constant as a function of ramp-length. The post-integration noise appears to decrease with smaller ramp-length, but the error in the determination also becomes bigger. Within 3σ this value is also constant.

The median value for the post-integration noise is 260 / 233 (-5) for detector 3 / 12 (at 0.2 pF), respectively. At a capacitance of 1.1 pF (using some files where the radiation was already operating) the post-integration noise is about 86 / 80 (-5) for detector 3 / 12, respectively.

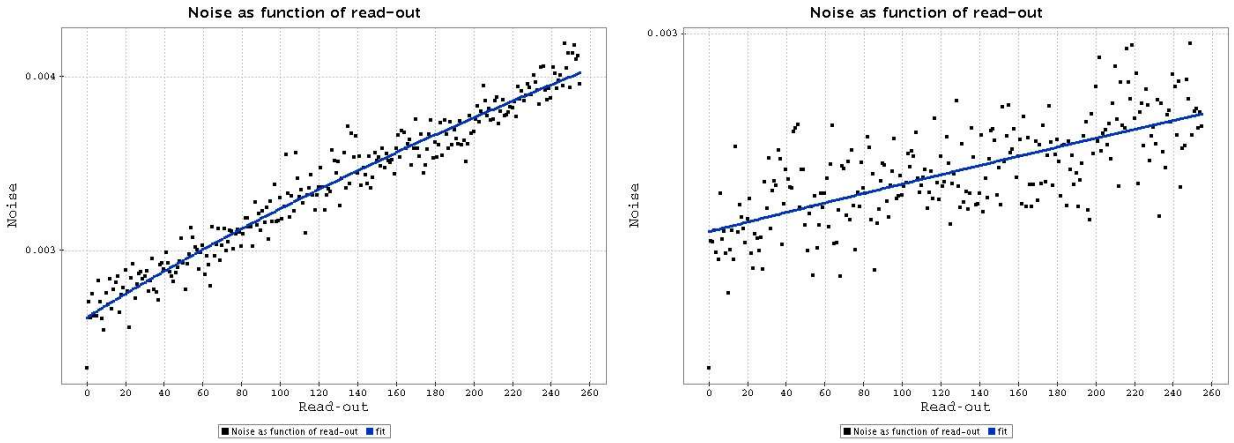

Figure 1: Noise as a function of read-out for detector 3 in files T185b70d10t1c02n256_#N_1.dat (left) and T185b20d10t1c02n256_#N_16.dat (right).

The analysis has been repeated by subtracting detector 0 for selected files. The results are listed and shown in Table 2 and Figure 2. The post-integration noise levels are reduced by 20-25%, the integrated noise levels by 5-10%.

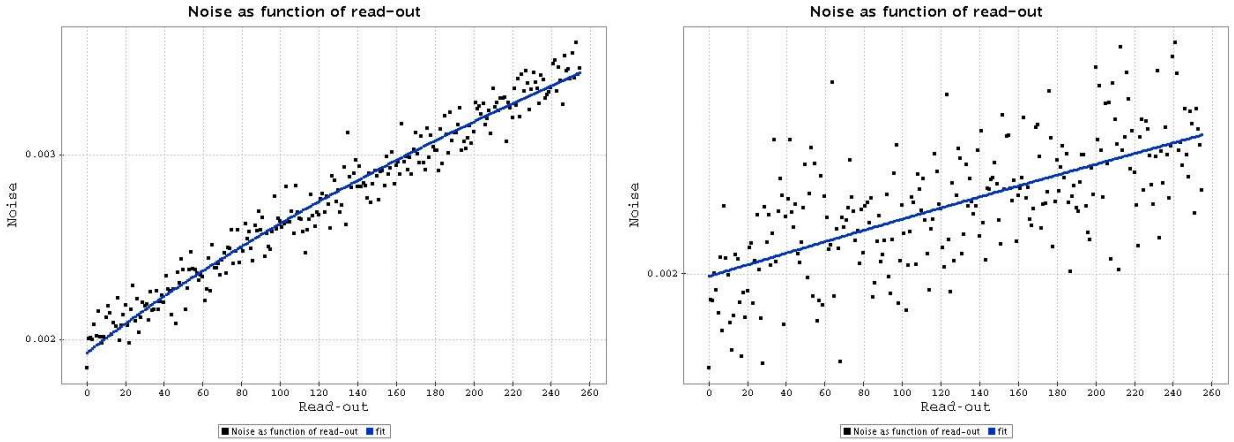

Figure 2: As figure 1 but *with detector zero subtracted*.

3. Overall shape of the ramps

The files of the pre-irradiation test with ramplength of 1 second have been fitted with the IMEC model of the ramps, as described in RD 3. To recall, the ramps are described as:

$$V(t) = V(0) + A\ (-1.0 + \exp(-t\ \zeta\ \omega) \times (\cosh(t\ \omega\ d) + (\zeta + \omega\ \tau)/d \times \sinh(t\ \omega\ d))) \tag{1}$$

with

$$d = \sqrt{\zeta^2 - 1}$$

where t represent time, and ω and ζ are known via the relations

$$\omega = 1.0/\sqrt{(C_\mathrm{f} + C_\mathrm{p})\ R_\mathrm{d}\ \tau_\mathrm{c}} \tag{2}$$

and

$$\zeta = \omega \times \frac{1}{2}\ (((1.0 + A)\ C_\mathrm{f} + C_\mathrm{p})\ R_\mathrm{d} + \tau_\mathrm{c}) \tag{3}$$

The parameters of the model (some of which are known) are therefore:

$V(0)$, Voltage at first read-out
A, amplifier gain
$C_{\rm f}$, feedback capacitance
$C_{\rm p}$, parasitic capacitance
$R_{\rm d}$, resistance of the detector, a proxy for the in-falling infra-red light
$\tau_{\rm c}$, time constant of the amplifier
τ, ad-hoc parameter, related to the "bump"
$V_{\rm b}$, bias voltage

It is also useful to define a *slope* (in units of V/s), as in the limit of infinite gain Equation (1) becomes

$$slope = \frac{dV(t)}{dt} = \frac{-V_{\rm b}}{C_{\rm f}\ R_{\rm d}} \tag{4}$$

In other words, $R_{\rm d}$ is fitted, and then *slope* is calculated according to Eq. 4.

Initially some trial runs were made with only the feedback capacitance and the bias value fixed at their known values and leaving the other parameters free. It sooned turned out that compared to the MPE April 2003 test data fitted in RD 3 the "bump" is essentially absent in the present data, and so τ can be fixed to zero.

After some further testing with 5 parameters left free ($V(0)$, A, $C_{\rm p}$, $R_{\rm d}$, $\tau_{\rm c}$), it seemed that typical values for the gain and parasitic capacitance are 150 and 0.5 pF, respectively, and these parameters were then fixed. Table 3 presents the results. In this, and the following, tables, there is listed the filename, the detector (always 3 or 12), the number of ramps actually fitted/ total ramps in the dataset/ number of "weird" ramps (i.e. high χ^2, or fit failure), and then the median value of the output parameters (in this case, $\tau_{\rm c}$, and $R_{\rm d}$ converted to a slope following Eq. 4), and the number of function calls [a measure of the effectiveness of the fitting], reduced χ^2 returned for the fitting assuming a weight per read-out of 10^6 (i.e. an "error" of 0.001 V), and the noise determined by fitting a Gaussian to the residuals between the data and the fit.

Although the fitting results are not very bad, there are nevertheless quite some cases where the fitting fail. Table 4 shows the results when $\tau_{\rm c}$ is fixed at 0.037, which is the median value listed in Table 3.

Note that all fits converged now that $\tau_{\rm c}$ is also fixed. Also note that the *slope* is the only free-parameter (next to V(0)). It is also noted that the χ^2, or standard deviation in the residuals, are low, and very similar, except in the case for a bias of 70 mV, where the fits are slightly poorer.

Tables 5 and 6 list the same results with A, $c_{\rm p}$, or $\tau_{\rm c}$ fixed at slightly different values. These attempt were made to improve the situation for the 70 mV bias case. The poorest fits are nevertheless always for the highest bias value, and in that case the parameters used in Table 6 are formally best.

Returning to the integrated noise listed in Table 1, Table 6 lists in the last columns the value of $\sigma_{\rm i}/\sqrt{-slope}$ which is quite constant. One interpretation is that this is related to the Poisson character of the integrated noise: $\sigma_{\rm i} \sim \sqrt{N_{\rm electrons}}$.

We would have liked to repeat the analysis for the integration capacity used in the majority of the radiation tests (which is 1.09 pF), but all tests with 256 read-outs have been taken with a capacitance of 0.23 pF.

Finally, Table 7 repeats Table 6 but with detector zero subtracted.

In Tables 8 there is, for the pre-irradiation data, listed the filename, and then for detectors 3 and 12 each, 5 columns with the median value of the *slope*, the standard deviation in the *slope*, the number of function calls, reduced χ^2 returned for the fitting assuming a constant weight per read-out of 10^6 (i.e. an "error" of 0.001 V), and the noise determined by fitting a Gaussian to the residuals between the data and the fit.

The last column list the (S/N) for both detector 3 and 12, defined as (S/N)= mean(-slope)/stdev(slope)* $\sqrt{n_{\rm slopes}}$. Some clear trends are obvious: in the pre-irradiation data the best (S/N) are achieved for (1) the highest bias tested, namely 70 mV, and (2) for the longest ramp-length of 1 second.

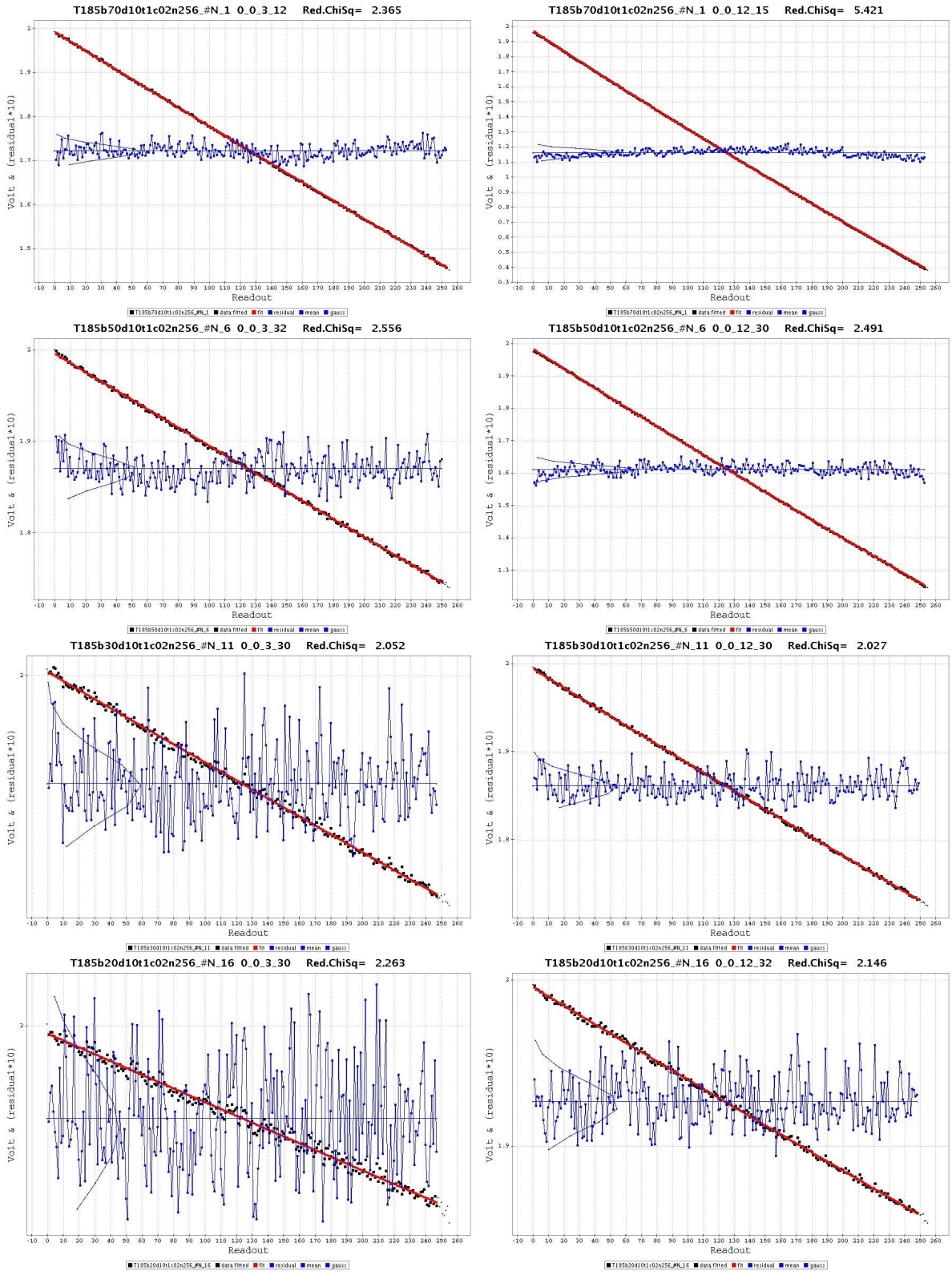

Figure 3: Selected fits for ramps of 1 second. Plotted are Volts versus read-out number. On the left for detector 3, on the right for detector 12. From top to bottom bias voltage of 70, 50, 30, 20 mV. The red points are the fits to the thick black points. Smaller black points are read-outs not considered in the fitting (last read-out, saturation, etc). The blue dots and line represent the residual, **TEN** * (observed-fitted), shifted to the mean voltage, indicated by the blue horizontal line. The other blue line is a Gaussian fit to a 9-bin histogram of these residuals. At the top of the plots are listed: the file name, the indices i_j_k_l, indicating the file number in the full list of files analysed, Module, Detector, Ramp, and the reduced Chi-square.

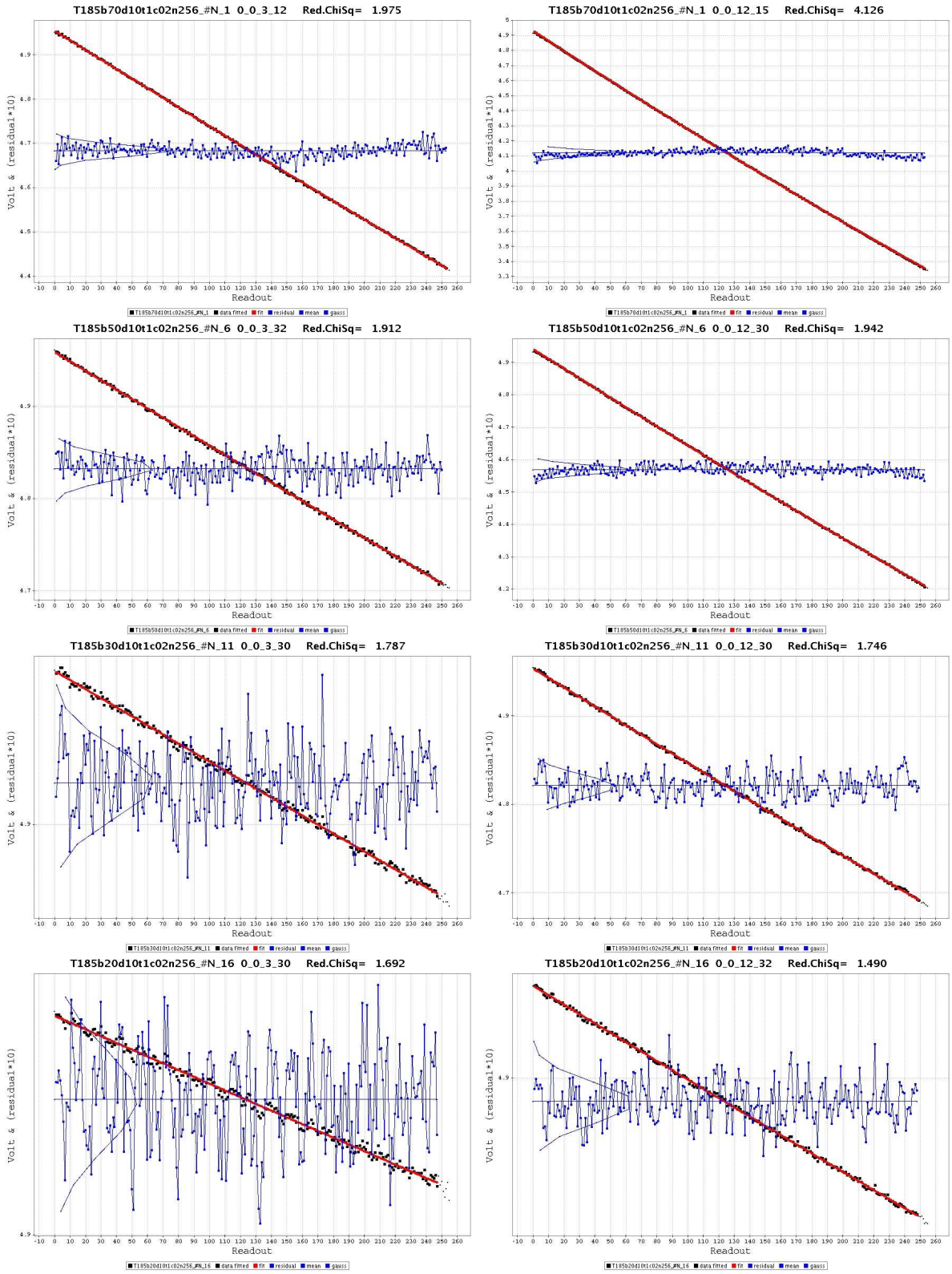

Figure 4: As previous figure with *detector zero subtracted*.

Table 1: Post-integration and integrated noise.

filename	detector	post-integration noise (10^{-5})	integrated noise (10^{-6})
T185b70d10t1c02n256_#N_1.dat	3	261.3 ± 1.5	191.4 ± 1.4
	12	152.8 ± 6.5	358.3 ± 1.9
T185b70d10t05c02n256_#N_2.dat	3	252.8 ± 1.7	162.4 ± 3.7
	12	213.4 ± 3.0	291.2 ± 3.0
T185b70d10t025c02n256_#N_3.dat	3	248.9 ± 2.6	159.7 ± 11.2
	12	232.5 ± 2.8	270.3 ± 6.7
T185b70d10t0125c02n256_#N_4.dat	3	274.4 ± 3.3	130.4 ± 38.7
	12	237.0 ± 3.8	270.9 ± 18.6
T185b50d10t1c02n256_#N_6.dat	3	262.6 ± 1.3	125.6 ± 1.8
	12	212.4 ± 2.3	223.4 ± 1.5
T185b50d10t05c02n256_#N_7.dat	3	264.5 ± 1.7	121.9 ± 5.0
	12	239.5 ± 1.9	208.1 ± 3.1
T185b50d10t025c02n256_#N_8.dat	3	251.1 ± 2.4	129.7 ± 12.5
	12	228.7 ± 2.3	194.7 ± 7.4
T185b50d10t0125c02n256_#N_9.dat	3	259.5 ± 3.8	190.1 ± 23.9
	12	235.6 ± 3.8	212.1 ± 2.3
T185b30d10t1c02n256_#N_11.dat	3	278.4 ± 1.3	100.8 ± 2.4
	12	247.4 ± 1.4	150.8 ± 1.6
T185b30d10t05c02n256_#N_12.dat	3	273.2 ± 1.4	91.3 ± 5.8
	12	247.9 ± 1.5	138.6 ± 3.5
T185b30d10t025c02n256_#N_13.dat	3	266.5 ± 2.5	137.4 ± 1.3
	12	236.1 ± 2.4	161.7 ± 9.7
T185b30d10t0125c02n256_#N_14.dat	3	279.1 ± 3.1	138.3 ± 3.5
	12	246.8 ± 3.3	180.3 ± 2.5
T185b20d10t1c02n256_#N_16.dat	3	252.2 ± 1.1	77.1 ± 2.5
	12	231.4 ± 1.2	102.5 ± 1.9
T185b20d10t05c02n256_#N_17.dat	3	261.9 ± 1.5	73.1 ± 7.1
	12	234.5 ± 1.4	114.6 ± 3.9
T185b20d10t025c02n256_#N_18.dat	3	254.1 ± 2.0	74.3 ± 18.6
	12	226.4 ± 2.0	116.0 ± 11.2
T185b20d10t0125c02n256_#N_19.dat	3	250.7 ± 3.0	174.0 ± 2.4
	12	230.8 ± 2.9	170.5 ± 2.2
T185b50d10t025c11n1024_#L_1.dat	3	86.1 ± 0.4	39.6 ± 2.7
	12	81.1 ± 0.5	43.3 ± 2.4
T185b50d10t025c11n1024_#L_9.dat	3	86.8 ± 0.6	54.5 ± 2.4
	12	80.6 ± 0.5	63.7 ± 1.6
T185b50d10t025c11n1024_#L_15.dat	3	78.2 ± 1.2	141.9 ± 1.8
	12	79.2 ± 0.7	87.0 ± 1.7
T185b50d10t025c11n1024_#L_19.dat	3	85.6 ± 0.7	81.9 ± 2.1
	12	72.1 ± 1.2	155.9 ± 1.5
T185b50d10t025c11n1024_#L_25.dat	3	83.7 ± 1.2	151.7 ± 1.9
	12	56.7 ± 3.7	217.4 ± 2.7
T185b50d10t025c11n1024_#L_29.dat	3	70.9 ± 3.4	204.4 ± 3.2
	12	35.2 ± 8.7	254.4 ± 3.3

Table 2: Post-integration and integrated noise, *with detector 0 subtracted*.

filename	detector	post-integration noise (10^{-5})	integrated noise (10^{-6})
T185b70d10t1c02n256_#N_1.dat	3	192.8 ± 1.5	178.6 ± 1.1
	12	$78.8 \pm 12.$	336.3 ± 1.9
T185b50d10t1c02n256_#N_6.dat	3	200.6 ± 1.1	120.3 ± 1.3
	12	157.3 ± 3.0	213.8 ± 1.5
T185b30d10t1c02n256_#N_11.dat	3	197.5 ± 1.1	81.4 ± 1.7
	12	184.2 ± 1.2	119.2 ± 1.2
T185b20d10t1c02n256_#N_16.dat	3	199.6 ± 1.1	62.3 ± 2.2
	12	187.1 ± 1.1	89.0 ± 1.5
T185b50d10t025c11n1024_#L_1.dat	3	106.5 ± 0.6	34.8 ± 4.7
	12	106.4 ± 0.6	23.8 ± 7.4

Table 3: Summary of fit results for detectors 3 and 12. $A \equiv 150$, $c_{\rm p} \equiv 0.5$pF. For the last 5 column the median values over all fitted ramps is listed.

filename	detector	#ramps fitted/total/weird	slope	$\tau_{\rm c}$	#calls	$\chi^2_{\rm red}$	noise
T185b70d10t1c02n256_#N_1.dat	3	242/256/2	-0.5696	0.143	12	2.84	0.001719
	12	256/256/0	-1.8819	0.413	14	5.07	0.002361
T185b50d10t1c02n256_#N_6.dat	3	221/256/24	-0.2648	0.033	24	2.63	0.001647
	12	256/256/0	-0.8416	0.530	13	2.29	0.001503
T185b30d10t1c02n256_#N_11.dat	3	237/256/17	-0.0956	0.035	20	2.47	0.001623
	12	195/256/37	-0.2830	0.033	30	4.05	0.001774
T185b20d10t1c02n256_#N_16.dat	3	253/256/2	-0.0497	0.039	18	2.46	0.001575
	12	226/256/26	-0.1468	0.105	16	2.30	0.001531

Table 4: Summary of fit results for detectors 3 and 12. $A \equiv 150$, $c_{\rm p} \equiv 0.5$pF, $\tau_{\rm c} \equiv 0.037$. For the last 4 column the median values over all fitted ramps is listed.

filename	detector	#ramps fitted/total/weird	slope	#calls	$\chi^2_{\rm red}$	noise
T185b70d10t1c02n256_#N_1.dat	3	256/256/0	-0.5668	10	2.72	0.001682
	12	256/256/0	-1.7702	13	5.42	0.002384
T185b50d10t1c02n256_#N_6.dat	3	256/256/0	-0.2658	11	2.31	0.001533
	12	256/256/0	-0.7992	11	2.46	0.001512
T185b30d10t1c02n256_#N_11.dat	3	256/256/0	-0.0958	10	2.32	0.001520
	12	256/256/0	-0.2852	10	2.29	0.001515
T185b20d10t1c02n256_#N_16.dat	3	256/256/0	-0.0498	9	2.30	0.001535
	12	256/256/0	-0.1460	10	2.26	0.001498

Table 5: Summary of fit results for detectors 3 and 12. $A \equiv 220$, $c_{\rm p} \equiv 0.8$pF, $\tau_{\rm c} \equiv 0.037$. For the last 4 column the median values over all fitted ramps is listed.

filename	detector	#ramps fitted/total/weird	slope	#calls	$\chi^2_{\rm red}$	noise
T185b70d10t1c02n256_#N_1.dat	3	256/256/0	-0.5613	10	3.18	0.001839
	12	256/256/0	-1.7188	13	5.01	0.002341
T185b50d10t1c02n256_#N_6.dat	3	256/256/0	-0.2640	11	2.36	0.001562
	12	256/256/0	-0.7845	11	2.66	0.001669
T185b30d10t1c02n256_#N_11.dat	3	256/256/0	-0.0954	10	2.32	0.001524
	12	256/256/0	-0.2820	9	2.38	0.001558
T185b20d10t1c02n256_#N_16.dat	3	256/256/0	-0.0496	9	2.31	0.001537
	12	256/256/0	-0.1447	10	2.24	0.001495

Table 6: Summary of fit results for detectors 3 and 12. $A \equiv 150$, $c_{\rm p} \equiv 2.0$pF, $\tau_{\rm c} \equiv 0.060$. For the last 4 column the median values over all fitted ramps is listed.

filename	det	fitted/total/weird	slope	#calls	$\chi^2_{\rm red}$	noise	$\sigma_{\rm i}/\sqrt{-slope}$ (10^{-6})
T185b70d10t1c02n256_#N_1.dat	3	256/256/0	-0.5915	11	2.72	0.001682	249
	12	256/256/0	-1.8509	14	5.29	0.002386	263
T185b50d10t1c02n256_#N_6.dat	3	256/256/0	-0.2772	11	2.32	0.001532	239
	12	256/256/0	-0.8347	12	2.42	0.001517	235
T185b30d10t1c02n256_#N_11.dat	3	256/256/0	-0.0999	10	2.32	0.001519	319
	12	256/256/0	-0.2977	10	2.29	0.001515	276
T185b20d10t1c02n256_#N_16.dat	3	256/256/0	-0.0519	9	2.31	0.001537	338
	12	256/256/0	-0.1524	11	2.26	0.001500	263

Table 7: As Table 6 but *with detector zero subtracted*

filename	det	fitted/total/weird	slope	#calls	$\chi^2_{\rm red}$	noise	$\sigma_{\rm i}/\sqrt{-slope}$ (10^{-6})
T185b70d10t1c02n256_#N_1.dat	3	256/256/0	-0.5928	11	2.31	0.001530	232
	12	256/256/0	-1.8522	14	4.71	0.002241	247
T185b50d10t1c02n256_#N_6.dat	3	256/256/0	-0.2777	10	1.83	0.001389	228
	12	256/256/0	-0.8353	12	2.02	0.001398	234
T185b30d10t1c02n256_#N_11.dat	3	256/256/0	-0.0991	10	1.80	0.001358	259
	12	256/256/0	-0.2969	10	1.77	0.001355	219
T185b20d10t1c02n256_#N_16.dat	3	256/256/0	-0.0509	9	1.84	0.001381	276
	12	256/256/0	-0.1514	11	1.74	0.001345	229

Table 8: Pre-beam data: Summary of fit results with Ramp6Model for detectors 3 (cols. 2-6) and 12 (cols. 7-11). Values between brackets are uncertain as not all ramps were fitted in the process.

Name	slope	STDDEV (slope)	calls	$\chi^2_{\rm red}$	noise (10^{-4})	slope	STDDEV (slope)	calls	$\chi^2_{\rm red}$	noise (10^{-4})	(S/N)
N1	-0.59147	0.00237	11	2.7	16.8	-1.85100	0.00581	14	5.3	23.8	3993/5097
N2	-0.59894	0.00294	10	2.6	16.0	-1.83525	0.00601	12	2.5	15.7	3259/4885
N3	-0.60467	0.00450	8	2.6	15.7	-1.85500	0.00808	10	3.1	17.6	2149/3673
N4	-0.61359	0.01046	7	3.0	17.1	-1.88870	0.01324	8	3.2	18.2	938/2282
N5	-0.62753	0.03207	6	4.6	22.4	-1.92120	0.03422	7	4.6	22.6	313/898
N6	-0.27723	0.00139	11	2.3	15.3	-0.83476	0.00313	13	2.4	15.2	3191/4267
N7	-0.27892	0.00203	10	2.3	15.2	-0.84109	0.00361	11	2.5	16.1	2198/3727
N8	-0.28192	0.00421	8	2.5	15.0	-0.85153	0.00517	9	2.5	15.7	1071/2635
N9	-0.28525	0.01052	7	2.8	16.1	-0.85746	0.01159	7	2.8	16.4	433/1183.
N10	-0.29254	0.03303	5	4.8	22.5	-0.86441	0.03246	6	4.6	23.3	141/426
N11	-0.09991	0.00100	10	2.3	15.1	-0.29770	0.00171	10	2.3	15.1	1598/2785
N12	-0.10005	0.00176	9	2.4	15.4	-0.29867	0.00220	9	2.3	15.0	909/2172
N13	-0.10178	0.00399	7	2.5	15.4	-0.30017	0.00444	8	2.4	15.1	408/1081
N14	-0.10281	0.01000	6	2.9	17.6	-0.30186	0.01043	7	2.8	15.5	164/463
N15	(-0.18)	(0.026)	6	4.8	20.6	-0.30835	0.03118	5	4.4	19.2	110/158
N16	-0.05189	0.00086	9	2.3	14.6	-0.15237	0.00116	11	2.3	15.0	965/2101
N17	-0.05193	0.00173	8	2.3	15.0	-0.15186	0.00200	9	2.3	22.0	480/1214
N18	-0.05278	0.00396	7	2.5	15.2	-0.15278	0.00403	8	2.3	15.2	213/606
N19	(-0.061)	(0.010)	6	3.3	17.9	-0.15004	0.01060	6	2.7	16.6	98/226
N20	(-)	-	-	-	-	(-0.183)	(0.029)	6	5.4	29.0	

4. files L1-L29, H3-H6, L93-L102

This section deals primarily with the data taken over a time span more than 2 hours under low proton flux (files T185b50d10t025c11n1024_#L_1.dat up to L_29, including T185b50d10t025c11n1024fl03_#L_10.dat and T185b50d10t025c11n1024fl03_#L_20.dat).

Each file consists of 1024 ramps of 0.25 seconds, with a bias value of 50 mV and 1.09 pF capacitance.

All 29 $\times$ 1024 ramps of detectors 3 and 12 have been fitted with the IMEC model with $R_{\rm p}$ (i.e. *slope*) as only variable. A simple edge-detection-algorithm was used to detect the strongest glitches. No correction for the glitch was attempted and so only the part of the ramp prior to the glitch is fitted.

Figure 5 shows selective fits to the ramps.

Figure 6-8 show *slope*, noise (i.e. the sigma of a Gaussian fit to the residuals between observed ramp and the fit to it), and reduced χ^2, as a function of "time".

Table 9 collects these results in quantitative form. The table also lists the standard deviation over the slopes. One iteration of sigma-clipping is performed where 5 sigma outliers are removed, in order to compute the listed values.

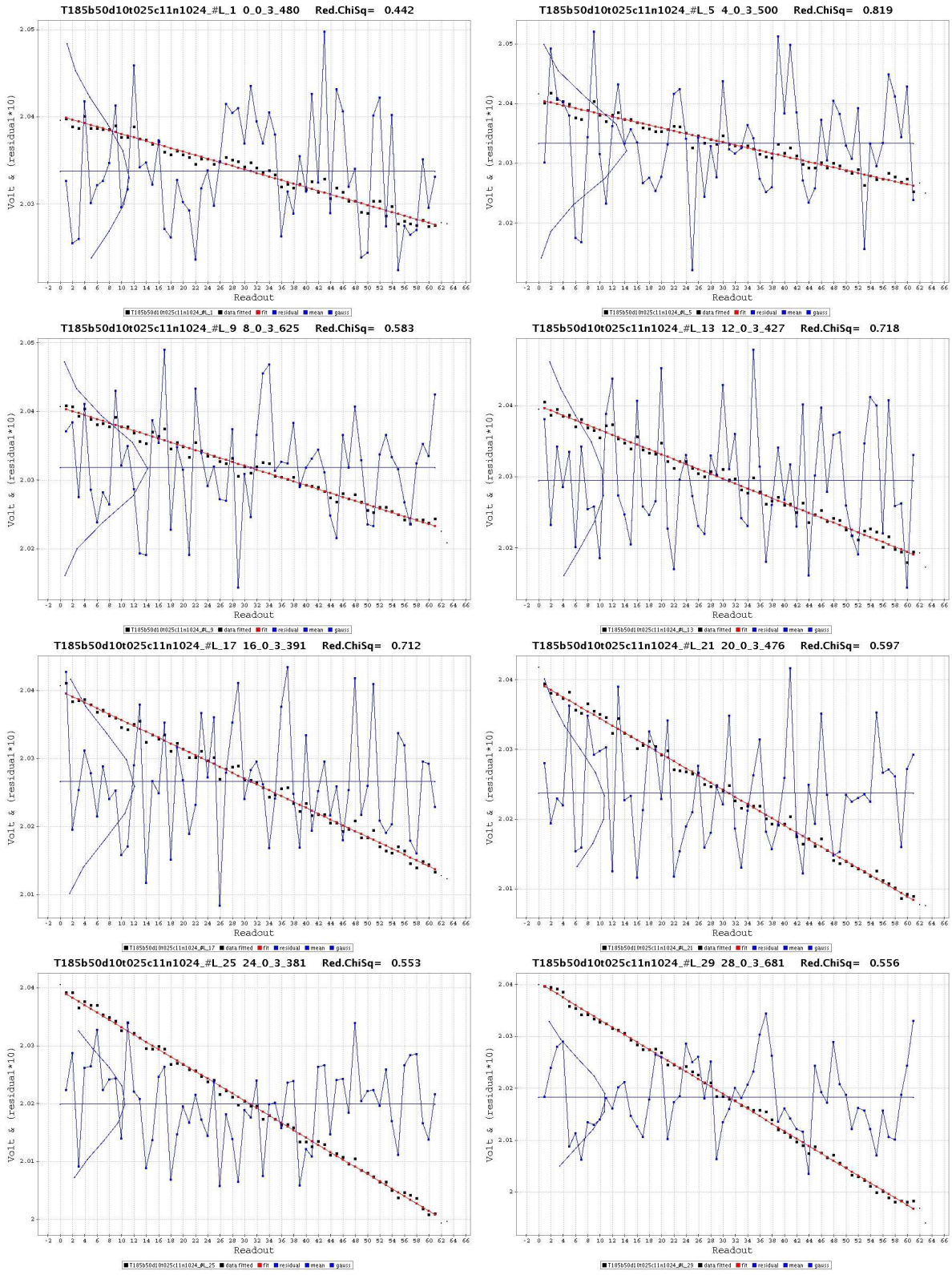

Figure 5: Selective fits for detector 3 of the long time series L_1 to L_29.

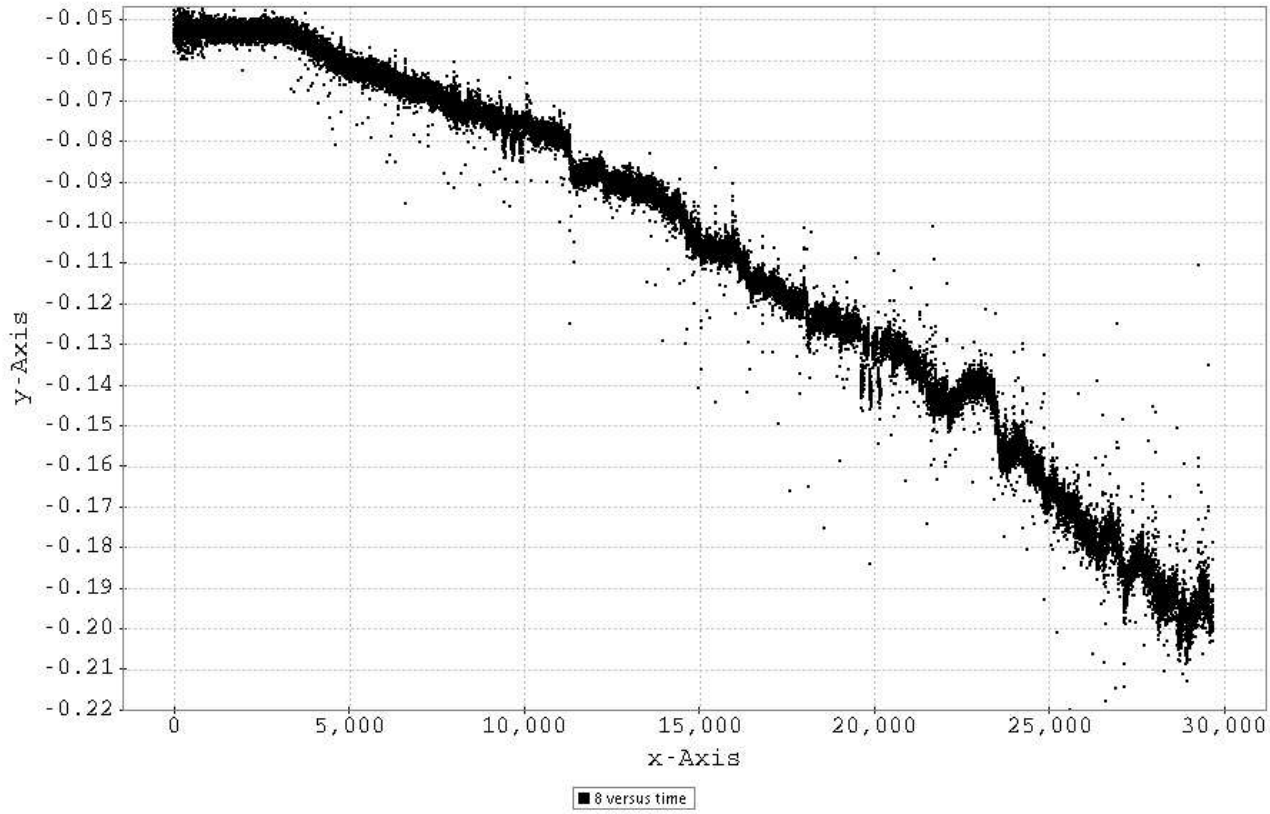

Figure 6: Slope (V/s) versus consecutive ramp number for detector 3 of the long time series L_1 to L_29. A similar plot is shown in RD1.

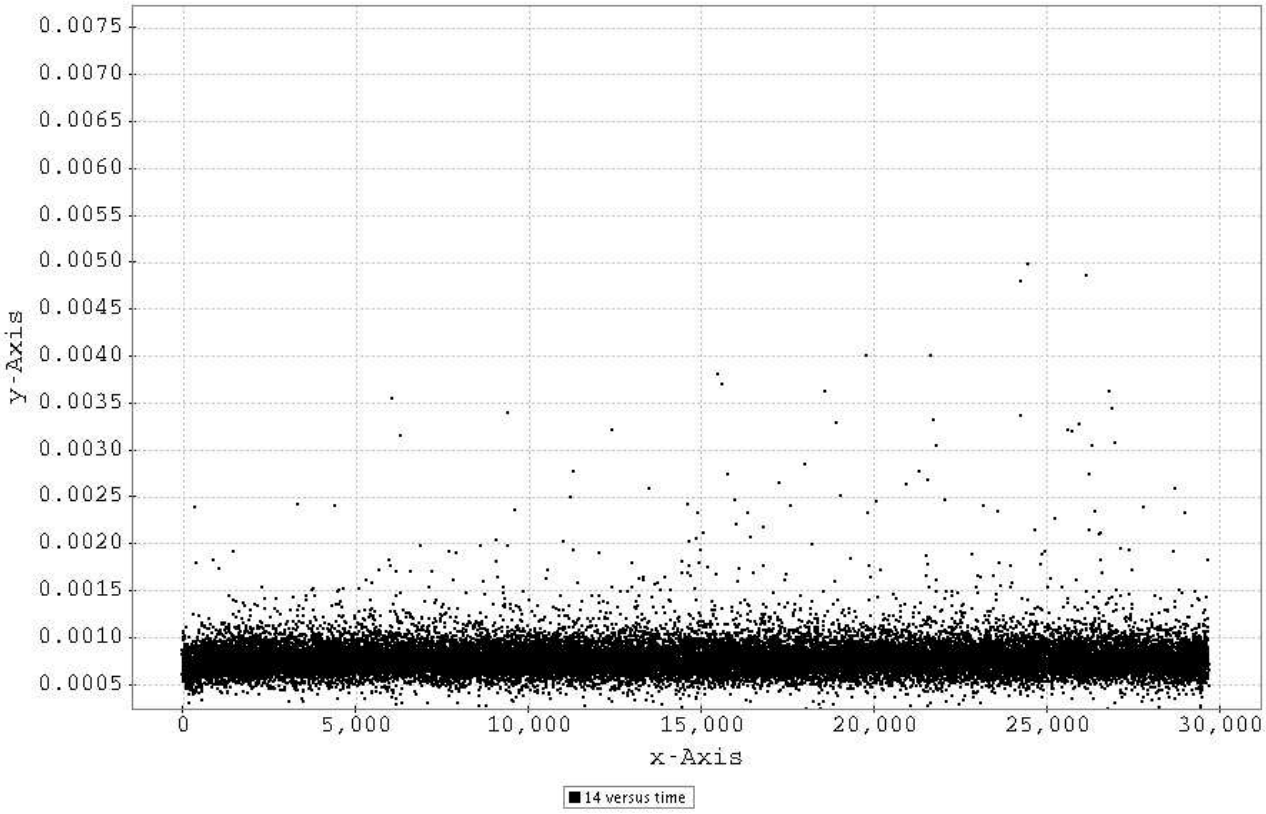

Figure 7: Noise (V) versus consecutive ramp number for detector 3 of the long time series L_1 to L_29. The quality of the fitting is essentially constant, but the number of outliers increases with time.

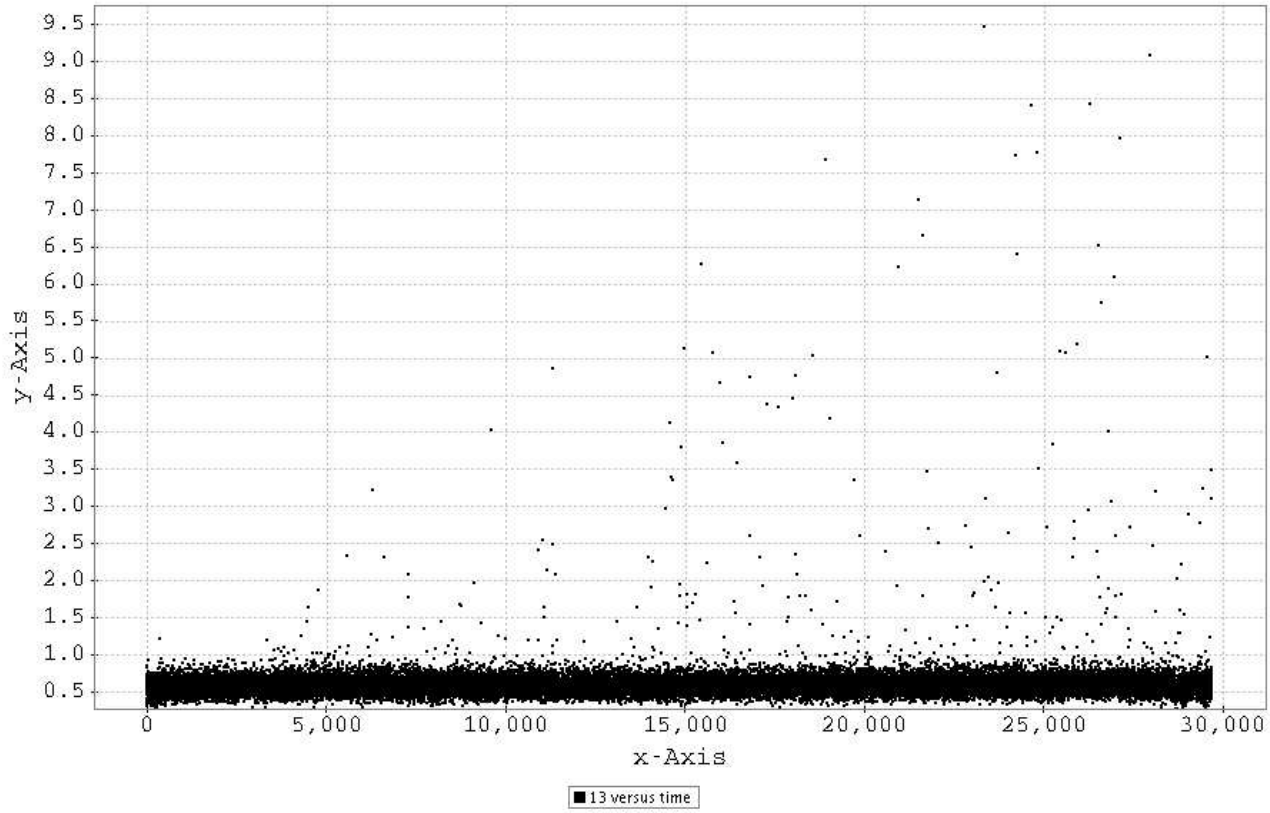

Figure 8: reduced χ^2 versus consecutive ramp number for detector 3 of the long time series L_1 to L_29.

Table 9: Summary of fit results with Ramp6Model for detectors 3 (cols. 2-6) and 12 (cols. 7-11).

filename	slope	STDDEV(slope)	#calls	$\chi^2_{\rm red}$	noise (10^{-4})	slope	STDDEV(slope)	#calls	$\chi^2_{\rm red}$	noise (10^{-4})
L1	-0.052907	0.00230	7	0.536	7.13	-0.15773	0.00226	6	0.521	7.06
L2	-0.052898	0.00141	7	0.564	7.35	-0.15775	0.00156	7	0.554	7.47
L3	-0.052837	0.00143	6	0.561	7.40	-0.15780	0.00151	7	0.549	7.36
L4	-0.054578	0.00201	7	0.564	7.51	-0.16083	0.00269	6	0.547	7.35
L5	-0.059855	0.00231	7	0.571	7.53	-0.16603	0.00216	6	0.558	7.43
L6	-0.063161	0.00169	7	0.576	7.55	-0.17179	0.00368	7	0.557	7.43
L7	-0.066805	0.00203	7	0.567	7.56	-0.18429	0.00514	7	0.555	7.31
L8	-0.069692	0.00222	7	0.564	7.42	-0.19338	0.00388	7	0.550	7.34
L9	-0.073342	0.00191	7	0.576	7.54	-0.20525	0.00191	6	0.560	7.41
L10	-0.076172	0.00303	7	0.577	7.45	-0.21307	0.00439	7	0.563	7.44
L11	-0.078379	0.00176	7	0.576	7.58	-0.22534	0.00313	7	0.563	7.50
L12	-0.087798	0.00227	7	0.569	7.39	-0.24649	0.00858	7	0.546	7.36
L13	-0.090705	0.00174	7	0.570	7.50	-0.26943	0.00291	7	0.552	7.40
L14	-0.093803	0.00258	7	0.570	7.45	-0.27849	0.00265	7	0.553	7.32
L15	-0.10365	0.00451	7	0.574	7.52	-0.27709	0.00276	7	0.553	7.39
L16	-0.10755	0.00267	7	0.572	7.55	-0.28767	0.00879	7	0.554	7.37
L17	-0.11544	0.00219	7	0.567	7.48	-0.30452	0.00516	7	0.549	7.39
L18	-0.12077	0.00360	7	0.568	7.38	-0.32113	0.00910	7	0.560	7.43
L19	-0.12478	0.00261	7	0.569	7.45	-0.33335	0.00487	7	0.559	7.40
L20	-0.13044	0.00545	7	0.588	7.50	-0.33088	0.00615	7	0.567	7.46
L21	-0.13402	0.00326	7	0.572	7.49	-0.34931	0.01644	7	0.567	7.45
L22	-0.14357	0.00347	7	0.583	7.63	-0.37546	0.01088	7	0.566	7.43
L23	-0.14074	0.00329	7	0.575	7.48	-0.39567	0.00760	7	0.577	7.53
L24	-0.15671	0.00358	7	0.587	7.52	-0.41139	0.00606	7	0.570	7.47
L25	-0.16631	0.00465	7	0.580	7.57	-0.43057	0.00706	7	0.562	7.53
L26	-0.17631	0.00531	7	0.583	7.67	-0.43885	0.01234	7	0.566	7.54
L27	-0.18203	0.00597	7	0.585	7.57	-0.44477	0.00615	7	0.575	7.59
L28	-0.18993	0.00524	7	0.578	7.46	-0.46070	0.01669	7	0.576	7.53
L29	-0.19559	0.00560	7	0.556	7.41	-0.49263	0.00780	7	0.549	7.22
L30	-0.20323	0.01012	7	0.584	7.62	-0.50311	0.01416	7	0.569	7.40
L31	-0.20794	0.01116	7	0.561	7.45	-0.50401	0.00678	7	0.550	7.33
H3	-0.94154	0.22728	9	2.623	10.2	-2.3539	0.57670	11	3.152	16.9
H4	-1.49025	0.15497	10	3.537	16.4	-3.9610	0.41970	12	5.303	21.9
H5	-1.65015	0.14578	10	3.527	13.7	-4.4679	0.31550	12	5.788	22.6
H6	-1.65245	0.16477	10	3.375	17.7	-4.6266	0.32110	12	6.195	22.9
L93	-0.55825	0.01288	8	2.124	13.5	-1.4678	0.02896	10	2.295	13.8
L94	-0.51559	0.01167	8	2.073	2.89	-1.4037	0.02647	10	2.188	13.6
L95	-0.23763	0.00767	8	2.109	13.4	-0.6160	0.01111	9	2.025	13.2
L96	-0.50649	0.01256	8	2.076	13.2	-1.3653	0.02409	10	2.151	13.7
L97	-1.05630	0.02206	9	2.324	3.46	-2.6269	0.04291	11	2.379	14.2
L98	-1.88820	0.04125	10	3.404	17.9	-4.6102	0.10814	12	4.457	19.5
L100	-0.22654	0.00749	8	2.041	13.1	-0.5501	0.01541	8	1.963	12.9
L101	-0.21777	0.00546	8	2.000	13.1	-0.5527	0.00778	8	1.914	12.8
L102	-0.21831	0.00538	8	1.989	12.8	-0.5457	0.00857	8	1.918	12.6

5. Glitches

As a start the script developed by Jürgen Schreiber based on the ISOPHOT deglitching was used (rampDeglitching.py / protonDeglitching.py).

Initially it was run with its main parameter set to *sigma1* = 6, but this resulted in too many false glitches in the pre-beam data, especially in the files of 0.125 seconds duration.

Finally a setting with *sigma1* = 8 was used in the analysis below[1]. Table 10 summarises the results for some series of files, separated for detectors 1-8 and 9-16. For the series of L4-L30 one sees that the number of glitches detected per unit time increases with time. This can be interpreted (see below) as that the expected glitch height increases when the responsivity increases. Although there are exceptions, the number of glitches is also larger for detectors 1-8 compared to 9-16.

Table 10 also includes the results from Angela Baier (AB) using the "SDE1'" method (see RD 4) for selected files.

Finally, Pierre Royers Q-method with two contrast functions and threshold1 = 0.4 (RD 4) was also used (PR). In that calculation glitches in the last-readout were, for some reasons, so heavily over represented that they were not considered in the glitch numbers listed in Table 10. As this effect was not seen in the results on the simulated data (RD 4), one may probably conclude that the last read-out is still affected by some systematic effect, although much smaller than seen in the old MPE 6-pack data.

Theory

Theoretically one expects that the glitch-height is given by (RD 5):

$$\Delta V[\mathrm{Volt}] = 0.1986\ \Delta E(\mathrm{MeV})\ \frac{R[\mathrm{A/W}]}{c_{\mathrm{f}}[\mathrm{pF}]\ \eta\ \lambda[\mu\mathrm{m}]\ E_{\mathrm{g}}[\mathrm{eV}]} \tag{5}$$

with R the Responsivity, E_{g} the energy loss per electron-hole pair produced (2.9 eV for Ge:GA), and η is the quantum efficiency (taken to be 0.3, Poglitsch, private communication).

For the tests with the stressed module one can take the wavelength to be 170 μm, and so one may expect the glitches to be of height:

$$\Delta V[\mathrm{Volt}] = 0.00134\ \Delta E(\mathrm{MeV})\ R[\mathrm{A/W}]/c_{\mathrm{f}}[\mathrm{pF}] \tag{6}$$

depending on the actual responsivity and capacitance used. As the responsivity is defined as:

$$R[A/W] = c_{\mathrm{f}}\frac{dV}{dt}/P \tag{7}$$

where P is the infalling power on a pixel ([1.7 and 5] 10^{-15} W for detectors 1-8 and 9-16, respectively). One has therefore as well:

$$\Delta V[\mathrm{Volt}] = 1.34\ \Delta E(\mathrm{MeV})\ \frac{dV}{dt}[\mathrm{V/s}]/P[10^{-15}\mathrm{W}] \tag{8}$$

The distribution of energy at the detector surface is listed in Figure 4 of RD 1 and may be approximated by a Gaussian with mean 17.5 MeV and spread 1.5 MeV. An alternative calculation is shown in Figure 3 of RD 1 and may be approximated by a Landau distribution (see RD 5) with mean E_{p} = 9.0 MeV and width R = 3.0 although this does not reproduce the short tail below 8 MeV. It is shown below (and it was already noted in the analysis of the March 2004 irradiation tests, see RD 5) that this has little to do with the distribution of deposited energy!

To compare theory with observations, the results of PRs algorithm on files L26-L29 and H5 are considered.

[1] and other parameters: *n_firstReject* = 1, *n_lastReject* = 1, *sigma2* = 2.0, *min_npix1* = 20, *min_npix2* = 20, *n_iterate* = 4, *n_lowReject* = 3, *n_highReject* = 3. Compared to previous work *n_firstReject* and *n_lastReject* have been set to 1 as the ramps have no bump. Schreibers script was slightly modifi ed to *not* subtract detector zero.

Table 10: Summary of glitches found. The number is for detectors (1-8)/(9-16), respectively.

filenames	time	number (JS)	number (AB)	number (PR)	comment
pre-beam, N1-N20	1920	2/2	-	-	c = 0.2 pF, 70-20 mV
pre-beam, flasher N21-N28	1882	5/1	-	-	
pre-beam, flasher N29-N39	2304	3/4	-	-	all in N36 with c = 0.1 pF
pre-beam, L1-L3	768	0/0	4/56	38/27	c = 1.1 pF, 50 mV
low proton flux, L4-L5	512	2/1	142/617	58/34	c = 1.1 pF, 50 mV
low proton flux, L6-L7	512	1/0	6/24	40/37	
low proton flux, L8-L9	512	8/4	15/21	61/52	
low proton flux, L10-L11	512	15/1	-	-	
low proton flux, L12-L13	512	13/7	13/30	74/43	
low proton flux, L14-L15	512	22/11	24/87	73/63	
low proton flux, L16-L17	512	30/17	43/179	84/64	
low proton flux, L18-L19	512	33/22	37/82	107/67	
low proton flux, L20-L21	512	58/30	-	-	
low proton flux, L22-L23	512	70/56	71/342	131/117	
low proton flux, L24-L25	512	74/44	85/227	164/87	
low proton flux, L26-L27	512	110/86	123/406	223/145	
low proton flux, L28-L29	512	148/101	141/276	265/184	
low proton flux, L30-L31	512	155/178	-	-	
high proton flux, H3	256	3138/3567	2849/3958	3051/2626	c = 0.2 pF, 30 mV
high proton flux, H4	256	3993/3909	3667/3920	3562/2886	
high proton flux, H5	256	3811/3662	3379/3461	3359/2711	
high proton flux, H6	256	3425/3425	3196/3291	3004/2501	
low proton flux, L93-94	512	114/106	151/1835	-	c = 0.2 pF, 30 mV
low proton flux, L95	256	19/17	51/367	51/51	c = 0.2 pF, 20 mV
low proton flux, L96	256	49/56	64/903	97/91	c = 0.2 pF, 30 mV
low proton flux, L97	256	174/110	249/1019	224/144	c = 0.2 pF, 40 mV
low proton flux, L98	256	199/175	1010/1103	273/202	c = 0.2 pF, 50 mV
low proton flux, L100-102	768	48/18	116/781	134/109	c = 0.2 pF, 20 mV

Let us first consider the files L26-L29. The black histogram in Figure 9 shows the distribution over glitch height of the 755 events. For this particular setting we know from the results on the simulated data that PR algorithm is about 80% complete with only 2% false detection.

Putting in numbers from Table 9 and the infalling power, we expect $\Delta V[\mathrm{Volt}] = 0.15\ \Delta E(\mathrm{MeV})$. In a numerical code we simulated (755/0.80) events distributed according to a Landau distribution, and made en eye-ball fit to the observations, represented as the red histogram. The parameters for the Landau distribution are a mean energy of 0.018 MeV, and a "material constant" (R) of 75. Figure 10 gives a representation of such a distribution in physical units.

This distribution is very different from the ones calculated for the energy at the detector surface, both in mean energy but also in width: the distribution of energy at the detector surface are rather narrow, while this is clearly inconsistent with the observed glitch height distribution.

The number of events observed in files L26-L29 corresponds to a rate of 755/ 1024 sec/ 0.24 sq.cm = 3.1 ($s^{-1}cm^{-2}$). Corrected for the detection efficiency of the detection algorithm a glitch rate rate of 3.9 ($s^{-1}cm^{-2}$) is derived. Since the beam was set to a nominal value of 10 protons ($s^{-1}cm^{-2}$) this seems to indicate that most protons that hit the crystal pass through cleanly, and/or that the number of secondaries generated is relatively small. Those protons that do not pass through cleanly, and/or the secondaries that are generated, deposit relatively small amounts of energy in the crystal.

This (apparent) low number of generated secondaries may be different in space as the physical 3D configuration of the instrument and spacecraft is very different from the set-up in Louvain-la-Neuve. In addition the energy distribution of

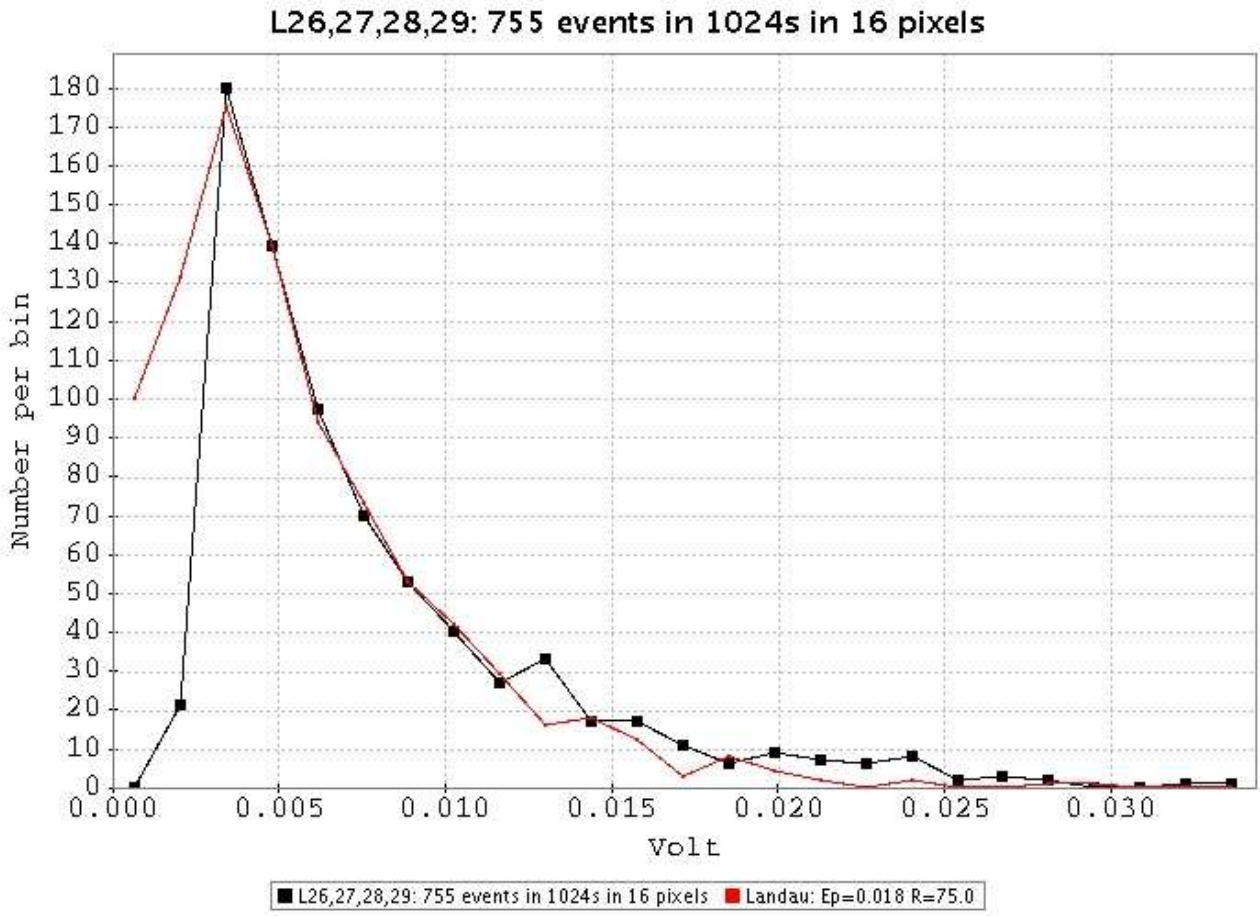

Figure 9: Distribution of glitches found by PR algorithm for files L26,27,28,29 (black histogram), and eye-ball fit of a Landau distribution of 1.25times as many events (red histogram).

normal space weather is different from the one in the cyclotron.

In a similar way file H5 was analysed. The number of events corrected for completeness is 6070/ 256 sec/ 0.24 sq.cm / 0.8 = 123 ($s^{-1}cm^{-2}$). The nominal value of the beam was set to 400 protons ($s^{-1}cm^{-2}$) The ratio 3.9/10 is very similar to 123 / 400 = 0.31.

Putting in numbers from Table 9 and the infalling power, we expect $\Delta V[\mathrm{Volt}] = 1.25\ \Delta E(\mathrm{MeV})$, and we repeated the numerical experiment. The result is shown in Figure 11. The mean energy of the Landau distribution is the same as for the low proton flux files, the distribution had to be made a bit wider than before (smaller R).

It is unclear why R should be different. The fit to the data is equally well when considering the glitches in detectors 1-8 and 9-16 separately.

Encouraging is that the glitch rates for the low and high proton fluxes are consistent with each other, and that the mean energy of the deposited energy is consistent between the 2 datasets considered. It implies that the theoretical framework (glitch height is proportional to slope) is a very good approximation.

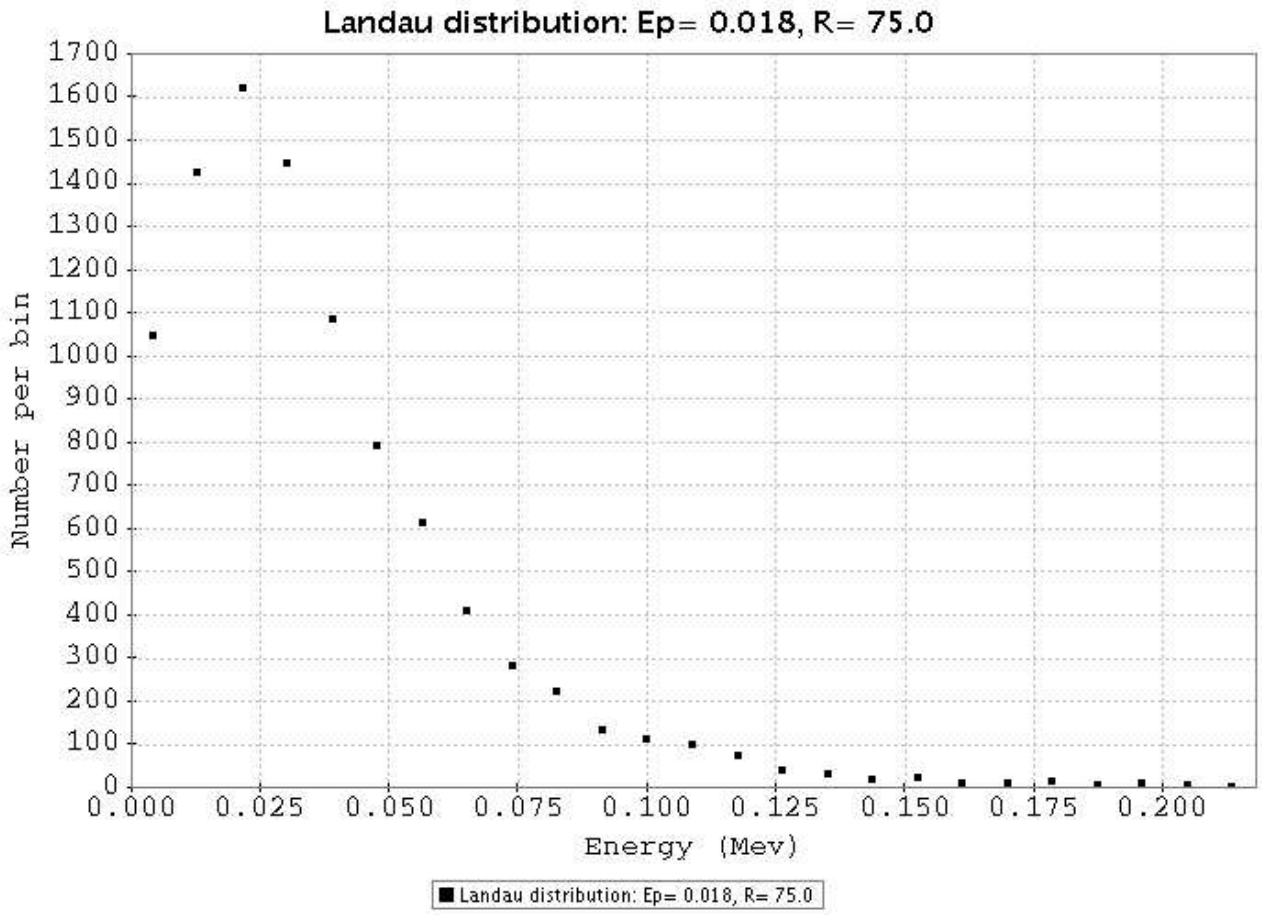

Figure 10: Distribution in Energy equivalent to the Landau distribution that fits the observed glitches in Figure 9. y-scale is arbitrary.

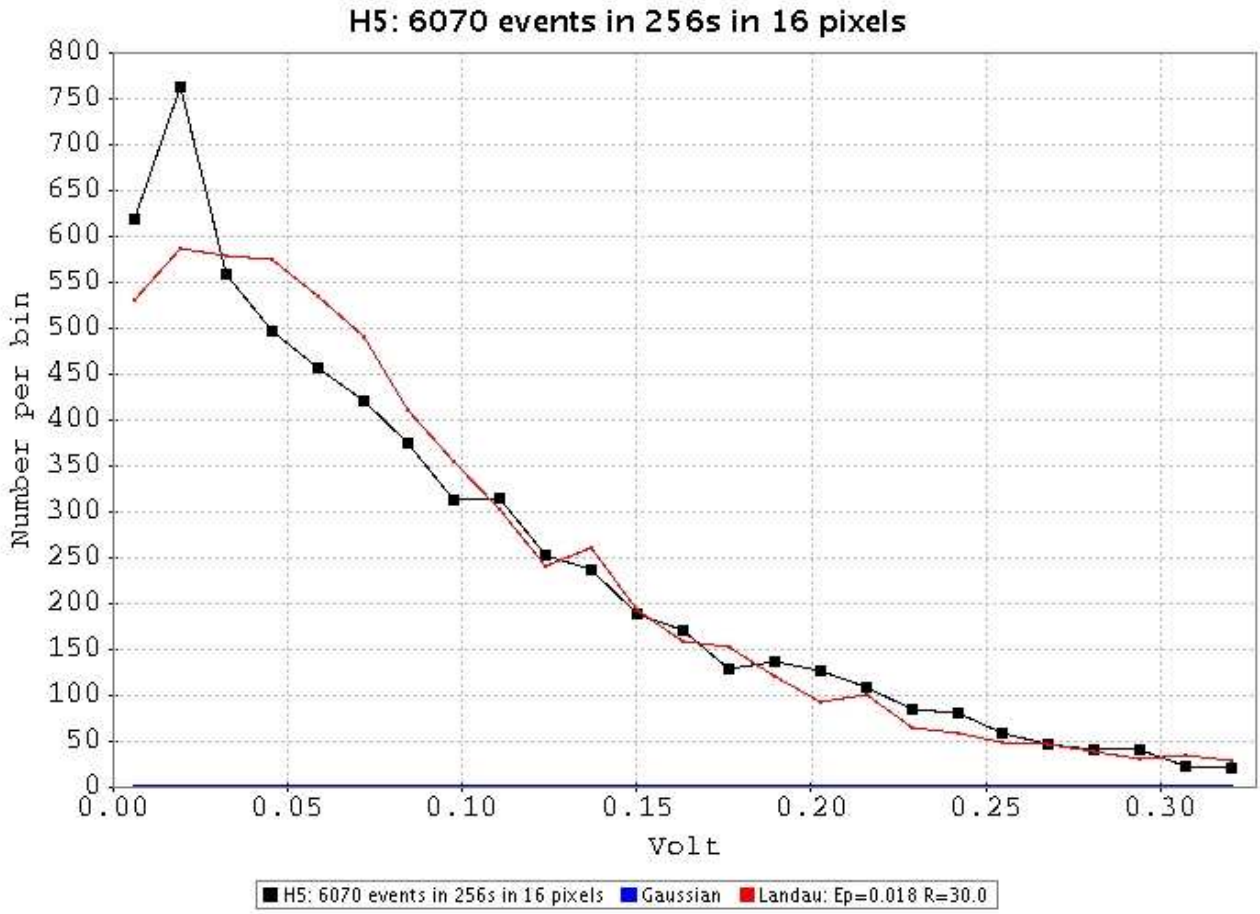

Figure 11: Distribution of glitches found by PR algorithm for file H5 (black histogram), and eye-ball fit of a Landau distribution of 1.25times as many events (red histogram).